Journal of Materials Science: Materials in Electronics (2019) 30:975–981
https://doi.org/10.1007/s10854-018-0366-5

Structural and magnetic properties of $CoMn_2O_4$ synthesized by auto combustion method

Rajeesh Kumar Narayanan Kutty[1] · Palanisamy Rupa Kasturi[1] · Jaya Jaganath[1] · Saravanan Padmanapan[2] · Yun Sung Lee[3] · Danielle Meyrick[4] · Ramakrishnan Kalai Selvan[1]

Received: 28 August 2018 / Accepted: 12 November 2018 / Published online: 20 November 2018

Abstract
Combustion synthesized cobalt manganite (CMO) was systematically studied for its structural and magnetic properties. X-ray diffraction (XRD) pattern with high-intensity peaks at appropriate positions revealed the formation of phase pure and highly crystalline CMO. The distorted tetragonal structure of the CMO unit cell suggested the presence of high spin (d^4) Jahn–Teller Mn^{3+} ions. X-ray photoelectron spectra (XPS) supported a mixed spinel with Co^{2+}, Co^{3+}, Mn^{2+} and Mn^{3+} cations. Electron microscopy confirmed the formation of submicron-sized CMO particles with well-defined lattice fringes, while low-temperature magnetic investigations revealed that the prepared CMO as a ferrimagnetic spinel due to the presence of uncompensated electronic states. The observed unsaturated magnetization, even at large applied fields, confirmed the high degree of spin-canting due to the existence of Yafet–Kittel spin arrangement.

1 Introduction

Spinel structured metal oxides are an interesting class of materials, which is known for their exciting magnetic properties and phase transition phenomena like Verwey transition, antiferromagnetic frustration, spin-glass state, commensurate-incommensurate phases, magneto-elastic and magnetodielectric coupling etc. [1–6]. These interesting properties naturally lead them to find application in multiferroics, spintronics, drug delivery etc. According to Bragg and Nishikawa, the AB_2O_4 structured spinel consists of a cubic closely-packed array of cations with more than one oxidation state occupying the tetrahedral (A) and octahedral (B) sites coordinated with oxygen atoms [7, 8]. The cationic distribution of spinel is represented as $(A_{1-x}B_x)[A_xB_{2-x}]O_4$, where x denotes the degree of inversion. When $x=0$, the formed one is a normal spinel and when $x=1$, an inverse spinel is formed. When x picks up an intermediate value between 0 and 1, a mixed spinel is obtained. The cation distribution plays a considerable role in altering the properties of spinel oxides. Site preference of cations depends upon (i) ion size, (ii) electronic configuration of ion and (iii) strength and symmetry of crystal filed at the site [9]. The dominant exchange interaction between and within the ocathedral (B) and tetrahedral (A) sub-lattices dictate the kind of magnetic ordering developed in the material. According to Neel's two sub-lattice model, A–B interactions are more stronger than A–A or B–B interactions. Owing to the inequality in the number of ions in the tetrahedral and octahedral sites and the strong exchange interaction between the sub-lattices leads to ferrimagnetic ordering [10].

Magnetic properties of the Mn-rich spinel oxides ($ZnMn_2O_4$, $CoMn_2O_4$, $FeMn_2O_4$) are explored relatively less when compared to that of Fe-rich spinel oxides (e.g. Fe_3O_4, $MnFe_2O_4$, $NiFe_2O_4$). This may be due to the requirement of the low-temperature magnetic measurement system and complex magnetic behaviour of Mn-rich spinels. Mn_3O_4 is a ferrimagnetic spinel evidencing triangular spin arrangement as suggested by Yafet and Kittel rather than obeying Neel's antiparallel spin [11]. When tetrahedral sites are substituted with non-magnetic ions like Mg or Zn, magnetic dilution effect can be observed resulting in weak exchange

✉ Ramakrishnan Kalai Selvan
selvankram@buc.edu.in

[1] Energy Storage and Conversion Devices Laboratory, Department of Physics, Bharathiar University, Coimbatore, Tamil Nadu 641 046, India

[2] Defence Metallurgical Research Laboratory, Hyderabad 500 058, India

[3] Faculty of Applied Chemical Engineering, Chonnam National University, Gwangju 500-757, South Korea

[4] Theranostics Australia, Richmond Quarter, 1 Silas St, East Fremantle, WA 6158, Australia

interactions [12, 13]. On the other hand, when Mn ions are substituted with magnetic ions like Co or Ni or Fe, the complex magnetic behaviour is observed which may be due to competing for exchange interaction among the lattice sites [14–17]. Thus there is a predominant necessity to understand this complex behaviour observed in the magnetic ion substituted Mn-rich spinels.

Herein, we report the synthesis of $CoMn_2O_4$ using the facile sol–gel auto-combustion method with glycine as fuel. $CoMn_2O_4$ is generally an inverse spinel oxide. Boucher at al. analysed the single crystal neutron diffraction data of $CoMn_2O_4$ and concluded that $CoMn_2O_4$ exhibited ferrimagnetism with canted spin arrangement [14]. A handful of reports have been available for this inverse spinel oxide synthesised using non-conventional routes followed by analysis of its magnetic properties [18–21]. Here, we have reported the synthesis of $CoMn_2O_4$ (CMO) using sol–gel auto-combustion method for analysing the magnetic properties. We have selected the sol–gel process due to better reported chemical homogeneity, high product purity and crystallinity, metastable phase stabilization and narrow particle size distribution [22]. It also possesses advantages like low external energy consumption and usage of relatively simple equipment. The sol–gel synthesized phase pure and highly crystalline CMO particles are systematically analysed to throw light on the variation in structural, morphological and magnetic properties in comparison with CMO synthesized using unconventional methods.

2 Experimental methods and materials

All reagents used were analytical grade and used as received without any further purification. For the preparation, starting precursors $Co(NO_3)_2{\cdot}6H_2O$ (Himedia, 99% pure), $MnCl_2{\cdot}4H_2O$ (Himedia 99% pure) and $C_2H_5NO_2$ (Merck, 99.5% pure) were chosen. Initially, stoichiometric amounts of highly pure $Co(NO_3)_2{\cdot}6H_2O$, $MnCl_2{\cdot}4H_2O$, glycine (rich e^- acceptor) crystals were dissolved in double distilled water individually and stirred for several minutes until a clear solution was obtained. Secondly, the dilute mixture of $Co(NO_3)_2{\cdot}6H_2O$ was added dropwise into the $MnCl_2{\cdot}4H_2O$ solution with gentle stirring. Finally, glycine was added dropwise, and the resulting solution was allowed to stir for another 15 min. The necessary quantity of concentrated ammonia solution was added to maintain solution pH of 7. The solution was heated to 80 °C until a pink colloidal gel, which was then fired at > 100 °C. The combustion process proceeded for approximately 5 min and yielded a grey–green foam, which was further heated inside the crucible until it was converted entirely into CMO powder. The CMO product was allowed to cool to room temperature and the obtained powder calcinated at 700 °C for 10 h. A blackish green coloured final product was attained.

Structural analysis was carried out using XPERT-PRO X-ray diffractometer. Morphological analysis by transmission electron microscopy and high-resolution TEM analysis was executed using JOEL JSM-2100 microscopy with an acceleration voltage of 200 kV. X-ray photoelectron spectroscopy was performed using ESCALAB 250, while magnetic property measurement system (MPMS) SQUID magnetometer was used to study the magnetic properties of the prepared material.

3 Results and discussion

X-Ray diffraction studies were carried out to investigate the formation and crystallinity of the prepared CMO (Fig. 1). Analysis of as-prepared CMO (Fig. 1a) illustrates that certain phases are not formed and are less crystalline prior to calcination. Following high-temperature calcination (Fig. 1b), numerous high and intense diffraction peaks are seen. The observed diffraction peaks at $2\theta = 18.40$, 29.46, 31.43, 33.05, 36.58, 38.92, 44.97, 51.87, 54.56, 59.17, 60.81 and 66.35 correspond to lattice planes (1 0 1), (1 1 2), (2 0 0), (1 0 3), (2 1 1), (0 0 4), (2 2 0), (2 0 4), (3 1 2), (3 2 1), (2 2 4) and (1 1 6), and evidence the purely formed high crystalline tetragonal CMO produced. These values agree with standard JCPDS card no. 77-0471, and no impurity peaks are observed.

The crystallite size of CMO, obtained using Scherrer's equation, was found to be 46 nm. The calculated lattice parameters a, c and the c/a ratio are a = 5.783 Å, c = 9.095 Å and 1.57, respectively, supporting the formation of CMO with distorted tetragonal symmetry. The tetragonal distortion validates the Jahn–Teller effect due to

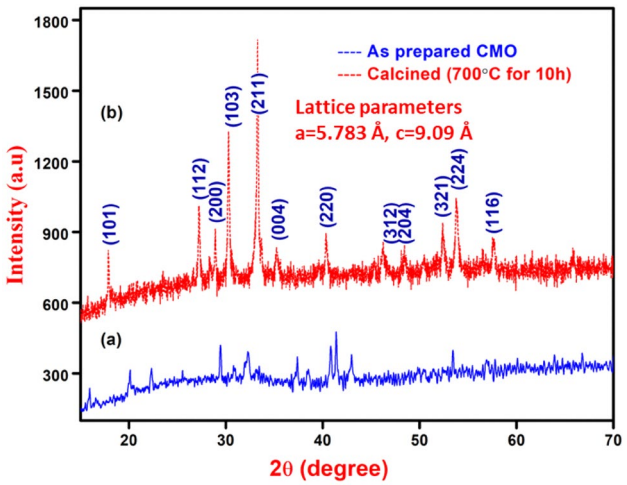

Fig. 1 XRD pattern of (a) as-prepared & (b) calcinated CMO

Mn^{3+} ions present in the octahedral sites [23]. According to the Jahn–Teller effect, there is a lift in the degeneracy of d-orbital states due to the crystal field of the ligand oxygen surrounding Mn^{3+} ions. The splitting of e_g doublets and t_{2g} triplets distorts the octahedral symmetry by leaving the $d_{x^2-y^2}$ orbital singly occupied and stabilizes the complex. The extra stability gained in such a way was compensated by elongation or compression of axial bonds of MnO_6 octahedron, thereby resulting in a distortion [24]. However, the obtained c/a ratio in the present work is lesser than hausmannite Mn_3O_4 (1.64). Also, an elongation along 'a' axis and compression along 'c' axis is observed in the prepared CMO in comparison with Mn_3O_4 [25]. It infers that there is a reduction in tetragonal symmetry, which must be due to the substitution of a few octahedral sites by Co^{3+} instead of Jahn–Teller Mn^{3+} ions. Similarly, Mn ions which could not occupy octahedral sites due to Co^{3+} occupation must have occupied tetrahedral sites by attaining 2 + states to maintain charge balance and thereby resulting in a mixed spinel.

To further confirm the presence of Co^{3+} and Mn^{2+} ions, in addition to Co^{2+} and Mn^{3+} ions, X-ray photoelectron spectroscopy (XPS) was employed. Figure 2a shows a representative survey spectrum of spinel CMO. The survey spectrum indicates the presence of the individual constituents of Co, Mn and O, as well as a small amount of carbon, used as a reference. The spectrum for Co 2p region is fitted using a Gaussian fit (Fig. 2b). The sharp peak located at the binding energy (E_B) of 780.5 eV is assigned to Co $2p_{3/2}$ while the peak around 796.3 eV is assigned to Co $2p_{1/2}$. The spin-orbital separation between Co $2p_{3/2}$ and Co $2p_{1/2}$ states is 12.8 eV. Satellite (sat) peaks also co-exist for cobalt; the peak located at E_B 786.1 eV is the satellite peak of Co $2p_{3/2}$, and that of Co $2p_{1/2}$ is situated at 802.9 eV. The peaks and their shake-up sats represent divalent and trivalent high spin Co [26]. The sat peak near 802.9 eV suggests the presence

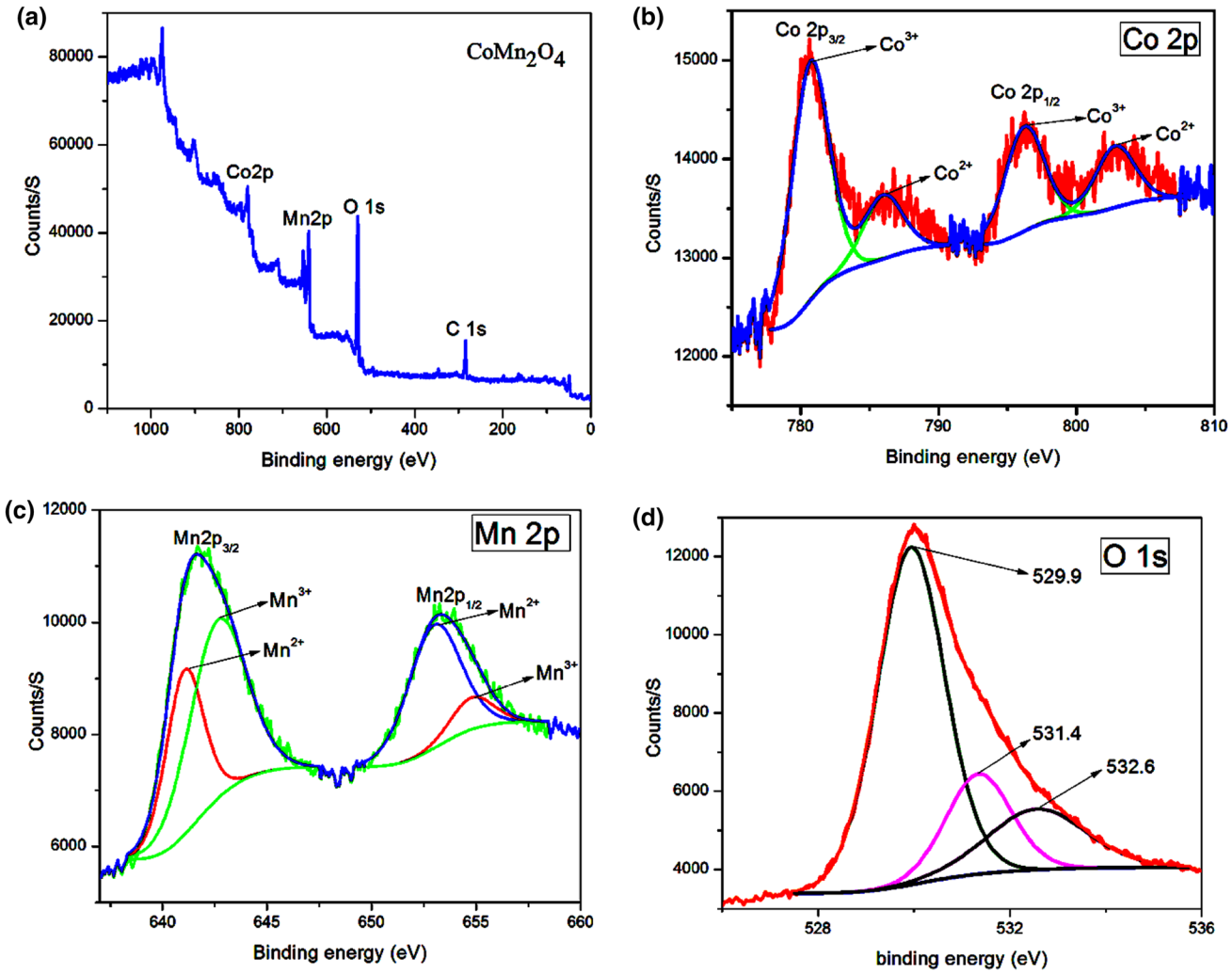

Fig. 2 XPS spectra of synthesized phase pure CMO, **a** survey spectrum, **b** Co 2p, **c** Mn 2p and **d** O 1s

of Co^{3+}, while that at 786.1 eV reflects the existence of Co^{2+}. This data suggest that the Co ions in CMO should be a mixed-valence with 2 + and 3 + states and the calculated Co^{3+}/Co^{2+} ratios for Co $2p_{3/2}$ and Co $2p_{1/2}$ states based on the area intensity are 0.993 and 1.008 respectively.

Similarly, Fig. 2c spectrum exhibit two prominent Mn 2p peaks. These are assigned to spin–orbit doublets Mn $2p_{3/2}$ and Mn $2p_{1/2}$ at the E_B of 641.6 eV and 653.4 eV. The high-intensity peak observed at 641.6 eV is mainly due to Mn^{3+} (Mn $2p_{3/2}$), while that at 653.4 eV is due to Mn^{2+} (Mn $2p_{1/2}$). The overall E_B separation between Mn $2p_{3/2}$ and Mn $2p_{1/2}$ states is found to be 11.8 eV, marking the evidence of cations in-between them [27]. After further refining, the parent Mn $2p_{3/2}$ and Mn $2p_{1/2}$ E_B peaks were convoluted into four different peaks. The deconvolution peak around 641.15 eV and 653.1 eV with an E_B separation of 11.9 eV can be assigned to the existence of Mn^{2+} cation, while the other peaks at 642.8 eV and 655.6 eV with an E_B separation of 12.8 are characteristic of the Mn^{3+} cation. The calculated Mn^{2+}/Mn^{3+} intensity ratios are 1.002, and 1.003 concerning Mn $2p_{3/2}$ and Mn $2p_{1/2}$ states determined to know about the quality of charge balance in the crystalline materials [28]. The de-convoluted O 1 s spectrum (Fig. 2d), shows a hump at 530.04 eV due to the oxygen ions (O^{2-}) of the metal oxides. The peak with E_B of 529.9 eV and 531.4 eV represents the metal oxygen bonds, while the peak at 532.6 eV evidences the low oxygen coordination with some defect sites within the material [18]. Hence, it is confirmed that Mn^{3+}, $Mn^{2+,}$ and Co^{3+}, Co^{2+} are coexisting in the synthesized spinel CMO structures.

The physical appearance and morphology of CMO were examined using traditional SEM and TEM techniques. Figure 3a-e shows, with a range of magnifications, the microstructural evolution of CMO calcined at 700 °C. Figure 3a shows the assembly of micron-sized grains of CMO with asymmetrical morphology while Fig. 3b, c show a few dark CMO particles crowded one upon another with average particle size around 150 nm. The exothermic reaction (combustion) during synthesis plays a vital role in the grain growth mechanism, due to which the sample shows microcrystallinity, with some sub-micron sized particles being trapped between larger particles with significant agglomeration [29, 30]. The lattice fringes observed by HRTEM (Fig. 3d) and the observed sharp spots in the SAED pattern (Fig. 3e) indicate the excellent crystallinity of the sample. Moreover, the d-spacing value between the lattice fringes found in Fig. 3d of (204) crystal plane is 0.181 nm, consistent with the XRD. EDAX analysis (Fig. 3f) was carried out

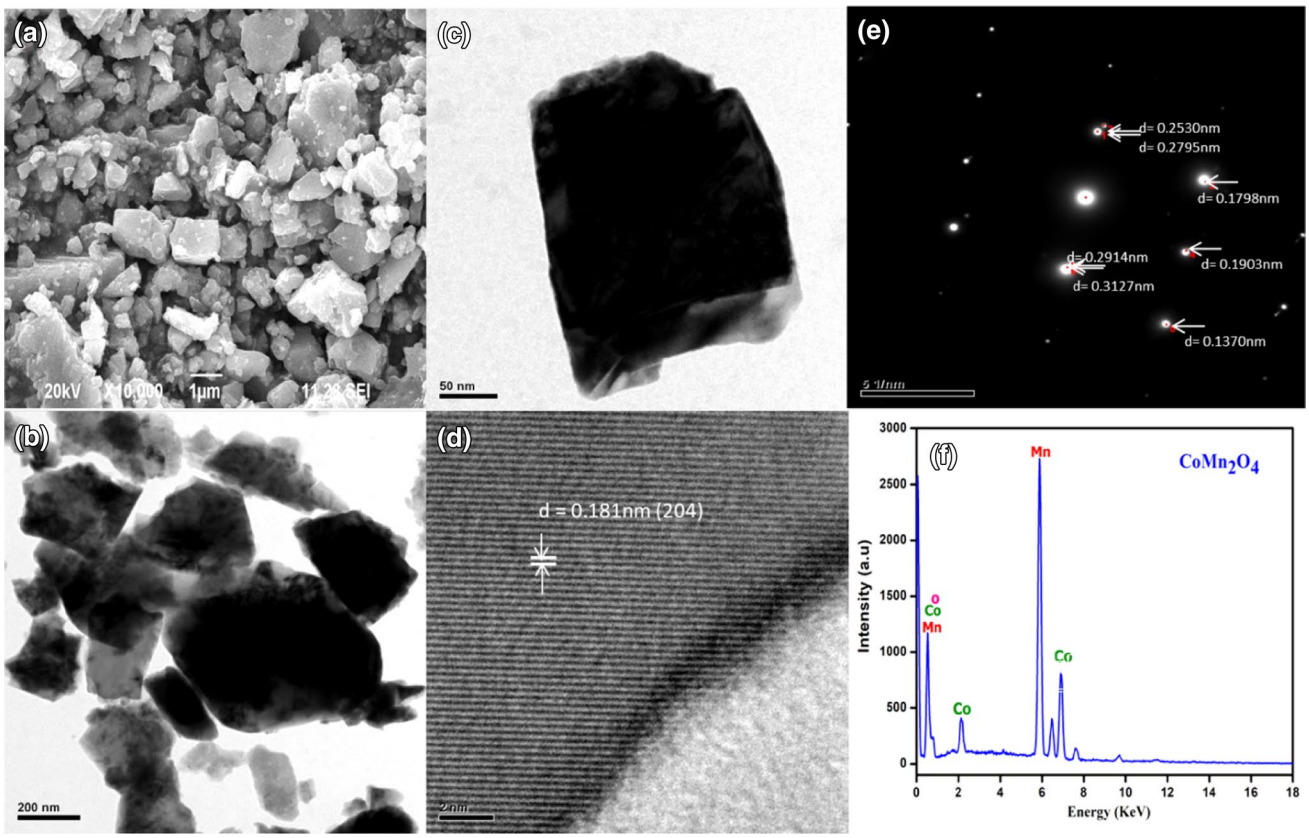

Fig. 3 **a–d** SEM, TEM and HRTEM images of prepared CMO. **e, f** SAED and EDAX pattern of CMO

to confirm the presence, and determine the wt% of, each of the constituent elements in the product. The weight% of Mn, Co, and O are about 62.056, 30.958 and 6.985, with corresponding atomic% of 54, 25 and 20 respectively. The Mn/Co atomic ratio determined by EDAX analysis is 2. The presence of other few humps may have originated from the copper grid and substrate.

The structural aspects of CMO induced our interest in studying its magnetic properties. The thermo-magnetic measurements for the calcined CMO obtained at an applied field H = 1000 Oe are shown in Fig. 4. It is observed that above 184 K, no change in magnetization occurs, indicating that the material is paramagnetic above that temperature. At 184 K, an increase in the magnetization was observed. This transition is considered as T_1. Mahata et al. had observed such a transition at 190 K and had suggested that this transition must be due to some impurity phases related to $Co_{3-x}Mn_xO_4$ [21]. Similarly, Habjinic et al. and Popovic et al. have reported similar transitions around 180 K which vanish with a decrement in particle size. In fact, this transition is a characteristic of bulk CMO [19, 20]. Similarly, At 74 K (T_2), another sharp transition with a very high

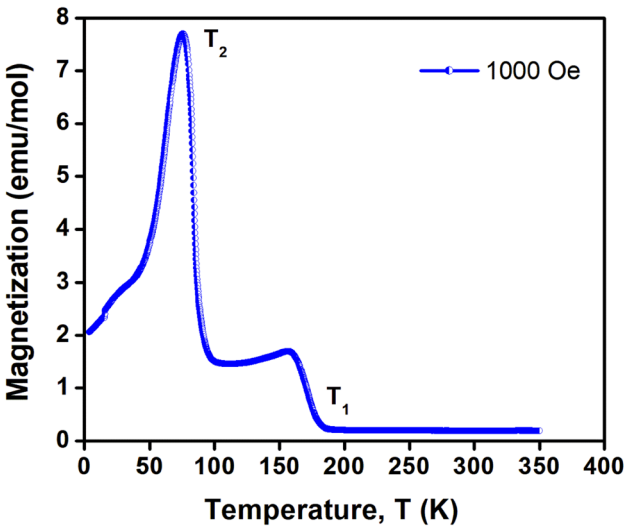

Fig. 4 Variation in Magnetization with the temperature at applied field H = 1000 Oe

magnetization was witnessed, which infers the occurrence of long-range magnetic ordering. As reported by Boucher et al. in his work on cobalt manganite single crystals, this transition must be due to the presence of Yafet–Kittel spin structures [14]. Below T_2, Mn^{3+} ions present in the octahedral sites must have attained a non-collinear triangular spin canting arrangement, which must have led to ferrimagnetic moments. Above T_2 there is a vanishing effect of these non-collinear moments among Mn^{3+} ions and thus a reduction in magnetization, as witnessed in M–T curve. Mn^{3+} ions present in the octahedral sites must be the sole reason for these Yafet–Kittel spin structures, as spins of Co^{2+}/Mn^{2+} occupying the tetrahedral sites were always collinear. In comparison with the other recent reports [20], a shift in T_2 towards lower temperature is observed in the present compound. The increased octahedral bond lengths and unit cell volume probably reduced the spin–spin interaction between metal centres, resulting in the shift of transition occurring at low temperatures (Refer Table 1).

To further understand the magnetic response in a wide range of field, isothermal magnetic studies were performed at different temperatures (4 K, 10 K, 100 K, 200 K, 300 K) within the magnetic field range of − 60 to + 60 kOe (Fig. 5). At 300 K (Fig. 5f), CMO exhibited paramagnetic behaviour. Bearing an equal number of spin up and spin down magnetic moments, net magnetization becomes zero due to the absence of exchange interaction. At 200 K, a very weak magnetization was observed at low applied fields (Fig. 5e). Even though no such indication was found in the M–T curve, irreversibility observed in the M–H curve at 200 K is a signature of antiferromagnetic interactions occurring in the compound. It confirms that the transition seen at 184 K (T_1) must be of anti-ferromagnetic origin. At 100 K (Fig. 5d), hysteresis loop with a reasonable coercivity (2850 Oe) and retentivity (5 emu/g) was obtained. However, coercivity and retentivity values were significantly increased with decrease in temperature (Fig. 5a–c). The measured coercivity values are 9800, 14,400, 15,980 Oe at 50 K, 10 K, and 4 K, respectively and these values are significantly higher when compared with other works reported using different methods [19, 21]. Such high values indicate the long-range ferrimagnetic ordering which occurs only in large-sized particles with

Table 1 Comparison of transition temperature T_2 with literature

Sample name	a (Å)	c(Å)	Cell volume (Å^3)	Method of preparation	T_2 (K)	Ref. no.
S800	5.7235	9.2622	303.64	Thermal decomposition of well-defined hetero-metallic complexes	82.3	[20]
S1000	5.7244	9.2701	303.76	Thermal decomposition of well-defined hetero-metallic complexes	78.9	[20]
CMO	5.783	9.095	304.16	Combustion method	74	Present work

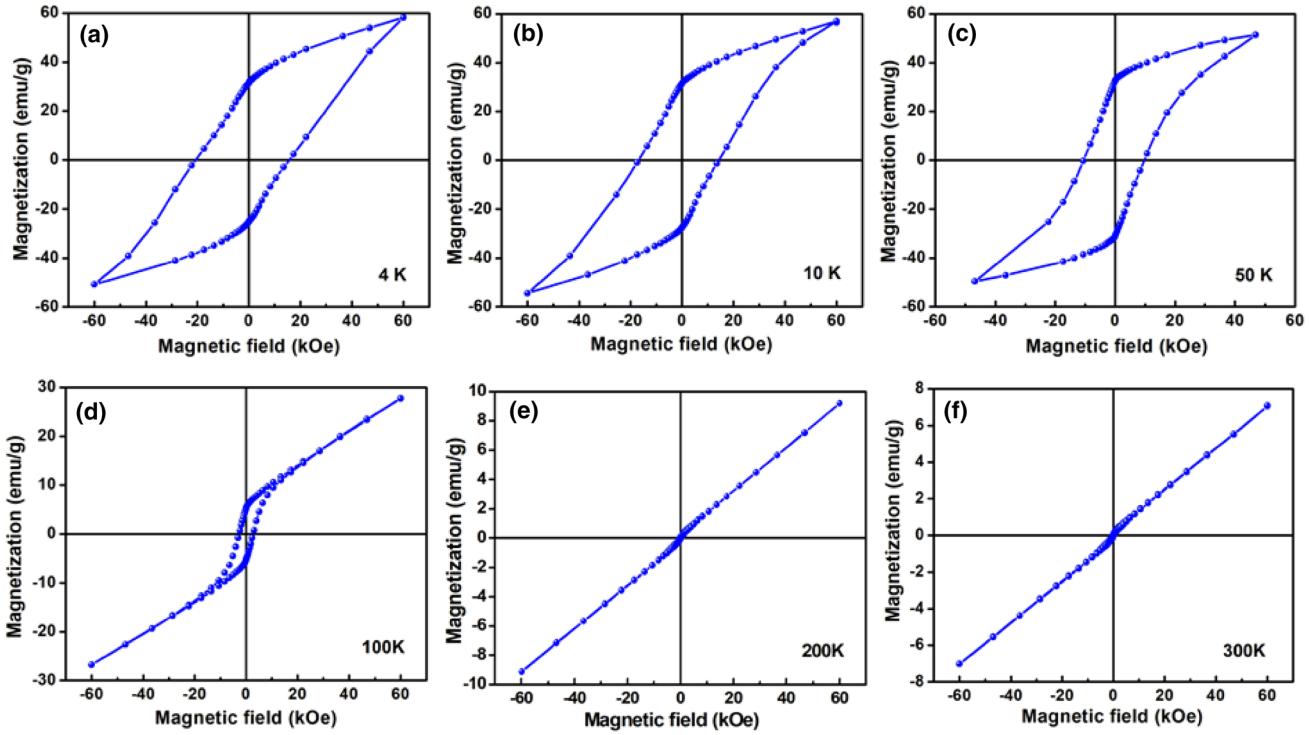

Fig. 5 Hysteresis loops of CMO measured at different temperatures

multi-grains formed due to agglomeration during synthesis. Ferrimagnetic behaviour in CMO is significantly attributed to uncompensated spin magnetic moments of Co^{2+}, Mn^{2+}, Co^{3+}, Mn^{3+} present in the lattice structure (observed in XPS results). Similarly, even at very high applied fields, no saturation magnetization was found in M–H loop. Unsaturated magnetization is a strong signature of spin canting effect due to antiferromagnetic interactions among the constituent ions in the lattice and is commonly observed in spinel materials like Mn_3O_4, $ZnMn_2O_4$, $MgMn_2O_4$ possessing Yafet–Kittel spin structures [13, 31, 32]. Thus, it can be concluded that the unsaturation of magnetization at higher fields and the observed transition at 74 K is due to a spin-canting effect caused by Yafet–Kittel spin structure of CMO. However, the Lotgering model which has successfully explained the exchange interactions and Yafet–Kittel spin happening in Mn_3O_4 and $ZnMn_2O_4$ could not be employed in CMO which may be due to complex exchange interactions among the constituent ions in the CMO lattice [32].

4 Conclusion

In summary, mixed spinel CMO particles have been prepared by a simple combustion method and were calcined at 700 °C for 10 h. The CMO particles obtained were highly crystalline and phase pure with tetragonal distortion in the structure. Comparatively, low c/a ratio indicate that the Co and Mn ions occupied both tetrahedral and octahedral sites and the prepared cobalt manganite is an inverse spinel. XPS spectra support the co-existence of Mn^{3+}/Mn^{2+} and Co^{3+}/Co^{2+}, and EDAX shows the atomic percentage of Mn, Co and O to be 54, 25 and 20 respectively. The morphological analysis showed irregular morphology and the particle size was estimated as 150 nm. The particle size plays a key role in the magnetic properties of this product. Magnetic studies confirm that the 184 K transition is a size-dependent one and is observed in our compound, owing to the larger particle size due to agglomeration at high temperatures during synthesis. The transition at 74 K supports the formation of Yafet–Kittel canted spin structures below that temperature. High coercivity values at lower temperatures suggest long-range ferrimagnetic ordering occurring in micro-sized CMO particles. Non-saturation of magnetization observed at 4 K, 10 K, and 50 K further substantiate the presence of antiferromagnetic interactions occurring in CMO lattice. These observations suggest the occurrence of spin canting and justify Yafet–Kittel arrangements in CMO. However, further research has to be carried out to arrive at an exact conclusion on 74 K transition.

Acknowledgements This work was supported by the National Research Foundation of Korea Grant funded by the Korean Government (MEST) (NRF-2011-C1AAA0010030538).

References

1. M. Iizumi, F. Koetzle, G. Shirane, S. Chikazumi, M. Matsui, S. Todo, Structure of magnetite (Fe_3O_4) below Verwey transition temperature. Acta Cryst. B **38**, 2121 (1982)
2. A.P. Ramirez, Strongly geometrically frustrated magnets. Annu. Rev. Mater. Sci. **24**, 453 (1994)
3. B. Chardon, F. Vigneron, Mn_3O_4 commensurate and incommensurate magnetic structures. J. Mag. Mag. Mat. **58**, 128 (1986)
4. Y. Ying, L. Wang, W. Li, L. Qiao, J. Zheng, J. Yu, W. Cai, L. Jiang, S. Che, L. Zhang, L. Ling, Spin glass in a geometrically frustrated magnet of $ZnFe_2O_4$ nanoparticles. J. Supercond. Nov. Magn. **31**, 3553 (2018)
5. S. Pal, S. Lal, Orbital and spin ordering physics of the Mn_3O_4 spinel. Phys. Rev. B **96**, 0751391 (2017)
6. R. Tackett, G. Lawes, B.C. Melot, M. Grossman, E.S. Toberer, R. Seshadri, Magnetodielectric coupling in Mn_3O_4. Phys. Rev. B **76**, 024409 (2007)
7. W.H. Bragg, The structure of the spinel group the crystals. Philos. Mag. **6**, 305 (1915)
8. S. Nishikawa, Structure of some crystals of spinel group. J. Mat. Phy. Soc. Japan **8**, 199 (1915)
9. A.H. Morrish, *The Physical Principles of Magnetism* (Wiley-IEEE Press, New York, 2001)
10. L.M. Neel, Properietes magnetiques des ferrites; ferrimagnetism et antiferromagnetism. Ann. Phys. **12**, 137 (1948)
11. K. Dwight, N. Menyuk, Magnetic properties of Mn_3O_4 and the canted spin problem. Phys. Rev. **119**, 1470 (1960)
12. L. Nadherny, M. Marysko, D. Sedmidubsky, C. Martin, Structural and magnetic properties of $Zn_xMn_{3-x}O_4$. J. Mag. Mag. Mat. **413**, 89 (2016)
13. A.B. Antunes. M. Bahout. O. Peña. B. Mehdaoui, G. Martínez, Magnetic properties of the spinel system $MgxMn_3$-xO_4. Bol. Soc. Esp. Ceram. Vidrio. **47**, 143 (2008)
14. B. Boucher, R. Buhl, M. Perrin, Magnetic structure of cobalt manganite by neutron diffraction. J.Appl. Phys. **39**, 632 (1968)
15. V. Baron, J. Gutzmer, H. Rundolf, R. Tellgren, The influence of iron substitution on the magnetic properties of hausmannite, $Mn^{2+}(Fe, Mn)_2{}^{3+}O_4$. Am. Mineral **83**, 786 (1998)
16. S. Nepal, Q. Zhang, S. Dai, W. Tin, S.E. Nagler, R. Jin, Structural and magnetic transitions in spinel $FeMn_2O_4$ single crystals. Phys. Rev. B **97**, 024410 (2018)
17. G.T. Bhandage, H.V. Keer, Magnetic properties of $ZnMn_2O_4$–$NiMn_2O_4$ system. J. Phys. C: Solid State Phys. **11**, L219 (1978)
18. H.T. Zhang, X.H. Chen, Size-dependent X-ray photoelectron spectroscopy and complex magnetic properties of $CoMn_2O_4$ spinel. Nanotechnology **17**, 1384 (2006)
19. J. Habjanic, M. Juric, J. Popovic, J. Molcanov, D. Pajic, 3D oxalate- based network as a precursor for the CoMn2O4 spinel: synthesis and structural and magnetic properties. Inorg. Chem. **53**, 9633 (2014)
20. J. Popovic, M. Juric, D. Pajic, M. Vrankic, J. Zavasnik, J. Habjanic, Effect of cation distribution and microstructure on the magnetic behavior of the $CoMn_2O_4$ oxide. Inorg. Chem. **56**, 3983 (2017)
21. P. Mahata, D. Sarma, C. Madhu, A. Sundaresan, S. Natarajan, $CoMn_2O_4$ spinel from a MOF: synthesis, structural and magnetic studies. Dalton Trans. **40**, 1952 (2011)
22. K.C. Patil, S.T. Aruna, T. Mimani, Combustion synthesis: an update. Curr. Opin. Sol. Stat. Mat. Sci. **6**, 507 (2002)
23. J.B. Goodenough, A.L. Loeb, Theory of Ionic ordering, crystal distortion and magnetic exchange due to covalent forces in spinels. Phys. Rev. **98**, 391 (1955)
24. J.D. Dunitz, L.E. Orgel, Electronic properties of transition metal oxides. J. Phys. Chem. Solids **3**, 20 (1957)
25. F. Bosi, U. Helenius, H. Skogby, Crystal chemistry of $MgAl_2O_4$–$MgMn_2O_4$–$MnMn_2O_4$: analysis of structural distortion in spinel- and hausmannite-type structures. Am. Mineral **95**, 602 (2010)
26. J. Li, S. Xiong, X. Lia, Y. Qian, A facile route to synthesize multiporous $MnCo_2O_4$ and $CoMn_2O_4$ spinel quasi-hollow spheres with improved lithium storage properties. J. Nanoscale **5**, 2045 (2013)
27. G. Yang, X. Xu, W. Yan, H. Yanga, S. Ding, Single-spinneret electrospinning fabrication of $CoMn_2O_4$ hollow nanofibers with excellent performance in Lithium ion batteries. Electrochim. Acta **137**, 462 (2014)
28. T.Y. Ma, Y. Zheng, S. Dai, M. Jaroniec, S.Z. Qiao, Mesoporous, $MnCo_2O_4$ with abundant oxygen vacancy defects as high performance oxygen reduction catalysts. J. Mater. Chem. A **2**, 8676 (2014)
29. P. Vigneshwaran, M. Kandiban, N. Senthil Kumar, V. Venkatachalam, R. Jayavel, Vetha Potheher I study on the synthesis and characterization of $CoMn_2O_4$ electrode material for supercapacitor applications. J. Mater. Sci.: Mater. Electron. **27**, 4653 (2016)
30. M.S. Park, J. Kim, K.J. Kim, J.W. Lee, J.H. Kim, Y. Yamauchi, Porous nanoarchitectures. Phys. Chem. Chem. Phys. **17**, 30963 (2015)
31. I.S. Jacobs, Evidence for triangular moment arrangements in $MO{\cdot}Mn_2O_3$. J. Appl. Phys. **30**, 301S (1959)
32. G. Srinivasan, M.S. Seeehra, Magnetic properties of Mn_3O_4 and a solution of canted spin problem. Phys. Rev. B **28**, 1 (1983)